Next Materials 11 (2026) 101665

Contents lists available at ScienceDirect

Next Materials

journal homepage: www.sciencedirect.com/journal/next-materials

Research article

Structure-property relationships in bio-based polyurethane/carbon nanotube composite coatings revealed by principal component analysis

Muhammad Abdurrahman Munir [a,*], David Fernando [b,c], Imam Shofid Alaih [d], Fitria Rahmawati [d], Abdul Rohman [b,c]

[a] Faculty of Resource Science and Technology, Universiti Malaysia Sarawak, Kota Samarahan, Malaysia
[b] Centre of Excellence, Institute of Halal Industry and Systems, Universitas Gadjah Mada, Yogyakarta 5528, Indonesia
[c] Department of Pharmaceutical Chemistry, Faculty of Pharmacy, Universitas Gadjah Mada, Yogyakarta 55281, Indonesia
[d] Research Group of Solid Chemistry and Catalysis, Chemistry Department, Faculty of Mathematics and Natural Sciences, Sebelas Maret University, Surakarta, Indonesia

ARTICLE INFO

Keywords:
Carbon nanotubes
Impedance
Polyurethane
Thermal stability
Principal component analysis

ABSTRACT

This study investigates the structural, thermal, morphological, and electrical properties of bio-based polyurethane (PU) composites reinforced with carbon nanotubes (CNTs). PU was synthesized using methylene diphenyl diisocyanate (MDI) and palm kernel oil-derived polyol, while CNTs were incorporated in varying concentrations (1 %, 2 %, 5 %, and 10 %) via a sonication-assisted solution casting method. The chemical structure and successful incorporation of CNTs were confirmed using Fourier Transform Infrared Spectroscopy (FTIR), revealing the preservation of the PU backbone and the presence of non-covalent interactions such as hydrogen bonding. Principal Component Analysis (PCA) of FTIR data demonstrated effective differentiation between PU and PU/CNT composites based on subtle changes in the fingerprint region. Field Emission Scanning Electron Microscopy (FESEM) confirmed a uniform and well-integrated dispersion of CNTs in the PU matrix, with minimal aggregation, supporting effective nanofiller incorporation. Thermal analyses using Thermogravimetric Analysis (TGA) and Differential Scanning Calorimetry (DSC) revealed that CNTs improved the thermal stability, delayed decomposition onset, and increased residual char content, particularly at 5–10 wt% CNT. These enhancements were attributed to CNTs' barrier effect and high thermal conductivity. Electrochemical Impedance Spectroscopy (EIS) further demonstrated a significant reduction in bulk resistance with increasing CNT concentration, confirming enhanced electrical conductivity and the formation of conductive networks. The PU/CNT composites exhibited characteristic impedance behavior in line with the Randles circuit model, supporting their potential for electrochemical applications. Overall, the results indicate that CNT-reinforced PU composites possess enhanced thermal, structural, and electrochemical properties, making them promising candidates for flexible electronics, electrochemical sensors, and anti-corrosion coatings.

1. Introduction

Carbon nanomaterial applications to amplify the polymer as a composite are attracting many researchers due to their abundant nature and sustainability, along with their provision of the intimate interface needed for outstanding properties [1]. Based on the dimensions of dispersed carbon nanomaterials, there are several types of polymer nanocomposites, such as reduced graphene oxide (rGO), which is categorized as a carbon-based nanofiller two-dimensional (2D), and other nanomaterials such as fullerene, carbon black, and carbon quantum dots (CQDs) that have unique particle forms, whereas the last type is carbon nanotubes (CNTs) that can be categorized as one-dimensional (1D). This type is divided into two, namely single-walled carbon nanotubes (SWCNTs) and multi-walled carbon nanotubes (MWCNTs) [2,3]. Carbon nanotubes (CNTs) are considered highly effective nanofillers due to their combination of structural and functional properties. Their exceptionally high aspect ratio and large specific surface area facilitate strong interfacial interactions with polymer chains, which improve stress transfer and enhance mechanical reinforcement [4]. Additionally, their intrinsic mechanical strength and stiffness contribute to significant improvements in toughness, tensile strength, and durability when incorporated into polymer matrices. CNTs also exhibit superior electrical and thermal

* Corresponding author.
E-mail address: mmabdurrahman@unimas.my (M.A. Munir).

https://doi.org/10.1016/j.nxmate.2026.101665
Received 13 August 2025; Received in revised form 8 September 2025; Accepted 26 January 2026

conductivity, enabling the development of multifunctional composites with improved electrical pathways and enhanced thermal management properties [5,6]. Moreover, the chemical stability and low density of CNTs make them attractive for lightweight and durable composite applications. Within CNT types, multi-walled carbon nanotubes (MWCNTs) are often preferred over single-walled carbon nanotubes (SWCNTs) because they combine better electrical conductivity, lower production cost, improved dispersibility in polymer matrices, and reduced cytotoxicity. These advantages have led to their broader application in polymer nanocomposites, particularly in contexts where cost-effectiveness, processability, and biocompatibility are critical [5,6].

To apply a specific composite, a specific polymer matrix plays a major role in obtaining satisfactory properties. Numerous polymer matrices have been studied. However, polyurethane (PU) has become the most famous and versatile polymer with a broad range of applications and properties [7,8]. Polyurethane is commonly fabricated by two major segments; the hard segment has thermodynamic stability owing to the link between the hydrogen bonds and urethane. In contrast, the other segment, called the soft segment, endows PU with biodegradability and flexibility [9]. Specifically, the hard domains act as physical crosslinking points, which enhance mechanical strength, stiffness, and thermal stability, while the soft domains provide elasticity, flexibility, and toughness. The degree of phase separation also governs critical properties such as the glass transition temperature, shape-memory performance, and solvent resistance. A higher extent of separation typically improves mechanical durability and thermal stability, whereas greater mixing between phases can enhance flexibility and processability [10]. The application of bio-based PU as a polymer matrix is due to environmental concerns, depletion of petroleum resources, and the cost of material for fabricating a polymer. Furthermore, natural polymers become a choice because they offer numerous advantages, such as being renewable, eco-friendly, biodegradable, biocompatible, and inexpensive [11]. Among numerous natural polymer studies, PUs are famous substrates for the development of numerous conductive fillers owing to their ease of fabrication and modification, outstanding mechanical properties, and long lifespan, which is very good for reducing environmental pollution and waste of resources [12].

Polymers are typically characterized by low electrical conductivity; however, their properties can be significantly enhanced by the incorporation of conductive fillers [13]. Various conductive fillers have been extensively studied, including boron nitride nanotubes [14], carbon nanotubes (CNTs) [15], carbon nanofibers [16], carbon fibers [17], carbon black [18], expandable graphite [19], graphene [20], graphene nanoplatelets [21], and graphite [22]. Among these, carbon nanotubes have garnered significant attention due to their exceptional properties, such as low mass density, high aspect ratio, excellent thermal conductivity, superior electrical conductivity, and remarkable mechanical strength [23].

Given these characteristics, the incorporation of CNTs into a polymer matrix is a highly effective strategy for enhancing electrical conductivity and modifying electrode properties. Polyurethane (PU), a versatile block copolymer comprising alternating soft and hard segments, serves as a promising matrix. The soft segment, often derived from polyols like palm kernel oil, and the hard segment, typically composed of diisocyanates, are connected through urethane linkages (-NH-COO-) [9]. PU's unique structural flexibility and tunable properties make it an ideal candidate for hosting conductive fillers.

This study explores the integration of CNTs as conductive nanofillers in a PU matrix, examining various concentrations to enhance composite conductivity and performance. It introduces a novel approach by applying PCA to FTIR data to detect absorbance differences and using TGA to assess thermal degradation. These techniques, alongside CNT incorporation, support the development of efficient, conductive polymer-based electrodes for advanced electrochemical sensors. This combined analysis highlights the study's innovation.

2. Experimental procedures

2.1. Materials

Polyurethane was synthesized by Munir et al. [24] using 4,4-diphenylmethane diisocyanate (MDI) with an NCO content of 32 % and palm kernel oil (PKO), which had a hydroxyl value (OHV) of approximately 370 mg KOH/g and a moisture content below 0.1 %. PT supplied both MDI and PKO. Chemie Mitra Indonesia. Carbon nanotubes (CNTs) and *N*,*N*-dimethylformamide (DMF) were procured from Sigma Aldrich Indonesia. All chemicals used in the study were of analytical grade to ensure experimental reliability. Solutions were prepared using deionized water and stored at 4 °C to maintain stability and prevent degradation during the experiments.

3. Fabrication of PU/CNT

In the initial step, varying concentrations of CNTs (1, 2, 5, and 10 wt %) were prepared and dissolved in dimethylformamide (DMF) within an Erlenmeyer flask. To achieve uniform dispersion of the CNTs, the mixture was subjected to sonication at 60 °C while being stirred magnetically. The sonicator's temperature was carefully regulated by adding water to maintain the temperature. The process continued until a dark, ink-like solution was formed, indicating complete dispersion of the CNTs. Subsequently, approximately 10 mL of polyurethane (PU) solution was added to the CNT dispersion, and the mixture was stirred until a homogeneous solution was obtained. The final solution was then subjected to an evaporation casting process to produce a PU/CNT composite film. This involved pouring the solution into a mold and removing the solvent by placing the cast in a vacuum oven at 60°C for 6 h. This method ensured the formation of a uniform and well-integrated PU/CNT film.

3.1. Investigation of morphological, thermal, mechanical, and electrical conductivity properties of PU/CNT composites

Before analysis, the PU/CNT films were conditioned for 24 h at room temperature to ensure equilibrium. **Surface Analysis**: The surface morphology of the PU/CNT composites was investigated using a Field-Emission Scanning Electron Microscope (FESEM, JSM-6510 LA), equipped with Energy-Dispersive X-ray (EDX) spectroscopy for elemental composition analysis. **Thermal Characterization**; **Thermogravimetric Analysis (TGA):** The thermal stability of the PU/CNT composites was assessed using a PerkinElmer Pyris TGA. Approximately 10 mg of the sample was cut, weighed, and analyzed. The temperature range was set from 40°C to 800°C at a heating rate of 25 °C/min under a nitrogen gas flow of 50 mL/min. Principal Component Analysis (PCA) is applied to derivative thermogravimetry (DTG) data to evaluate thermal degradation differences between PU, PU/CNT, and CNT. The analysis is performed using Orange software version 3.36.1. Demsar et al., [25]. **Differential Scanning Calorimetry (DSC):** A PerkinElmer Pyris DSC was employed to study the thermal transitions. Approximately 10 mg of PU/CNT was cut, weighed, and sealed in aluminum pans. The sample was heated from 25°C to 150°C at a rate of 20 °C/min, held for 3 min, and then rapidly cooled to −100°C for 2 min. A second heating cycle was conducted from −100°C to 200°C at the same rate. The glass transition temperature (T_g) was determined from the inflection point in the heat capacity curve. **Chemical Characterization**: The chemical structure of the PU/CNT composites was analyzed using Fourier Transform Infrared (FTIR) spectroscopy (Thermo Scientific Nicolet iS10) with a Diamond Attenuated Total Reflectance (DATR) accessory. Functional groups were examined to verify the successful fabrication of PU/CNT composites: The -NH, -CH, -NCO, and -C═O were considered in the PU, where the $-NH_2$, $-NO_2$, and $-SO_3H$ were for the CNT. Principal component analysis (PCA) was employed to analyze the difference in absorbance at specific wavelengths for PU/CNT, PU, and MDI. The heatmap generated by the

MetaboAnalyst 6.0.0 software was used to visualize the results [26,27]. **Mechanical**: Tensile tests were conducted using an Instron 5566 universal testing machine following ASTM D638 (Standard Test Method for Tensile Properties of Plastics). Polyurethane films and polyurethane composites containing various concentrations of carbon nanotubes were cut into dumbbell-shaped specimens with dimensions. The tensile properties of the polyurethane films were measured at a strain rate of 10 mm/min using a 5 kN load cell. **Electrical Conductivity Analysis**: The electrical properties of the PU/CNT composites were investigated using Electrochemical Impedance Spectroscopy (EIS) with an Electrochemical Workstation (Sebelas Maret University, Indonesia). A three-electrode setup was used, such as PU/CNT (working electrode), platinum wire (auxiliary electrode), and Ag/AgCl (reference electrode). Measurements were conducted at room temperature under open-circuit potential (OCP). The frequency range was 10 MHz to 10 kHz with an amplitude of 10 mV. Data analysis was performed using the *ZView Analyzer* software to interpret impedance and resistance profiles.

4. Results and discussion

Fourier Transform Infrared Spectroscopy (FTIR) was utilized to investigate the chemical structure and to confirm the successful synthesis of both polyurethane (PU) and polyurethane/carbon nanotube (PU/CNT) composites, as illustrated in Fig. 1. The analysis focused on identifying key functional groups characteristic of the polyurethane (PU) backbone, which are critical for elucidating the chemical interactions between the PU matrix and carbon nanotubes within the composite structure. These functional groups serve as spectral markers for assessing molecular compatibility, dispersion quality, and potential bonding mechanisms between the matrix and fillers [28]. A total of twenty distinct absorption peaks were detected, corresponding to molecular vibrations attributed to PU-CNT, pure PU, or methylene diphenyl diisocyanate (MDI). The detailed peak assignments and their interpretations are summarized in Table 1.

Notably, the characteristic absorption band observed around ~3200 cm^{-1} corresponds to N–H stretching vibrations of urethane amide groups, confirming the presence of urethane linkages formed during polymerization [30]. Absorption bands near ~2900 cm^{-1} are attributed to aliphatic C–H stretching, commonly originating from polyol and polyethylene glycol (PEG) segments. A key observation is the absence of the isocyanate (-N = C═O) stretching band typically expected around ~2270–2400 cm^{-1}. This absence indicates complete consumption of isocyanate groups through reactions with hydroxyl groups from the polyol and PEG, confirming the formation of a fully crosslinked polyurethane (PU) network [31].

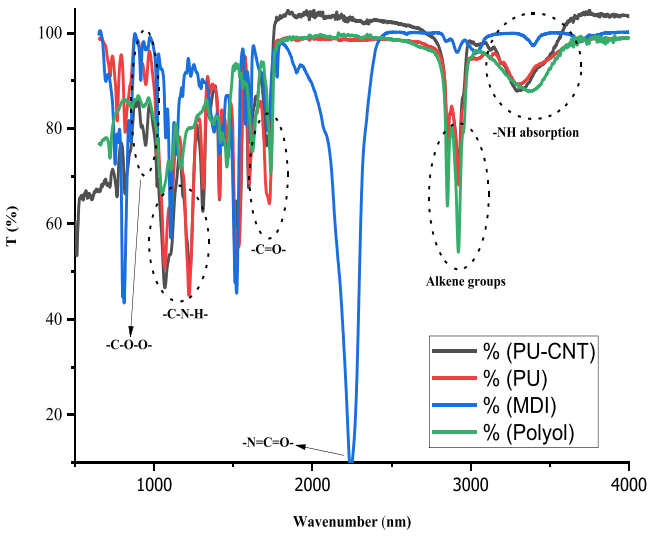

Fig. 1. FTIR spectrum of PU/CNT, PU, MDI, and Polyol.

Additional absorption bands around ~1300 cm^{-1} are attributed to carbamate (-C–NH) functionalities, while peaks near ~1100 cm^{-1} are indicative of C–O–C stretching vibrations, characteristic of ether linkages within the polyether soft segments, consistent with PU synthesized using methylene diphenyl diisocyanate (MDI) and palm kernel oil-based polyester polyol. These spectral features support the expected chemical architecture of the synthesized PU matrix. Importantly, no absorption was detected near ~1690 cm^{-1}, the region typically associated with C═O stretching of urea linkages. This absence suggests that side reactions with moisture, often leading to urea formation, were effectively minimized during synthesis [32].

The incorporation of carbon nanotubes (CNTs) did not introduce any new covalent bonding features, as the FTIR spectra of PU/CNT composites closely resembled those of neat PU. This suggests that CNTs were physically embedded in the matrix or engaged in weak non-covalent interactions. However, subtle variations in the intensity of N–H and C–O–C absorption bands may imply the presence of hydrogen bonding or secondary physical interactions between PU chains and the CNT surface, which is consistent with previous findings on CNT-polymer composites [33].

Single-walled carbon nanotubes (SWCNTs) are known to interact more strongly with the carbonyl (C═O) groups of polyurethane-amide (PUA) than with the amide nitrogen. This preferential interaction disrupts the typical inter- and intra-molecular hydrogen bonding network within the PU matrix, effectively blocking these interactions and altering the polymer's microstructure [34]. These subtle yet significant interactions are detectable through attenuated total reflectance Fourier transform infrared (ATR-FTIR) spectroscopy, which reveals changes in peak intensities rather than the emergence of new functional group bands, suggesting physical rather than covalent bonding between PU and SWCNTs [35].

Furthermore, to quantitatively validate these spectral differences, ATR-FTIR data were further analyzed using Principal Component Analysis (PCA). Absorbance values from twenty characteristic peaks were used as variables to differentiate among four sample groups: PU, PU-CNT, and pure methylene diphenyl diisocyanate (MDI) (Fig. 2a). PCA converts the 20 chosen variables into a new array of Principal Components (PC1 to PC20), with each component representing a linear amalgamation of the original absorbance values. The components are then sorted according to the variance they account for in the dataset, with PC1 explaining the most and PC20 the least. Thus, the PCs serve not merely as mathematical abstractions but also hold structural importance. The PCA results clearly distinguish the MDI sample, primarily due to the presence of the isocyanate (-N = C═O) stretching band at 2241 cm^{-1}. This peak serves as the dominant contributor to Principal Component 1 (PC1), with an eigenvalue of 0.89529, highlighting its strong influence in sample separation. Meanwhile, the 753 cm^{-1} peak contributes significantly to Principal Component 2 (PC2), with an eigenvalue of 0.57575, further assisting in differentiating the spectral profiles of PU-based materials.

Further analysis, excluding MDI, reveals that FTIR combined with Principal Component Analysis (PCA) effectively differentiates between PU and PU-CNT samples (Fig. 2b). The primary distinction lies along Principal Component 1 (PC1), where the most significant spectral contributor is the peak at 753 cm^{-1}, associated with an eigenvalue of 0.57447. This peak, located in the fingerprint region of the spectrum, appears to be sensitive to subtle structural changes induced by carbon nanotube incorporation. The observed separation suggests that CNTs influence hydrogen bonding within the PU matrix, leading to alterations in vibrational modes, particularly in the fingerprint region, without the emergence of new functional groups. These spectral modifications reflect changes in molecular interactions, likely driven by physical or secondary bonding between CNTs and PU chains.

Beyond the fingerprint region, several other spectral regions exhibited notable differences between PU and PU-CNT composites, as

Table 1
Infrared Spectra Interpretation of PU-CNT, PU, and MDI [29].

Wavenumber point (cm^{-1})	Functional group interpretation	Vibration mode	Intensity	Wavenumber range reference (cm^{-1})	Compound
3397	Primary and secondary amines and amides (N-H)	Stretching	Medium	3500–3100	PU, PU-CNT
3303	Primary and secondary amines and amides (N-H)	Stretching	Medium	3500–3100	PU, PU-CNT
3007	Alkene C-H	Stretching	Strong	3100–3000	PU, PU-CNT
2922	Aliphatic alkane (C-H)	Stretching	Strong	3000–2850	PU, PU-CNT
2853	Aliphatic alkane (C-H)	Stretching	Strong	3000–2850	PU, PU-CNT
2241	Isocyanate (-N = C═O)	Asymmetric stretching	Strong	2276 – 2240	MDI
1728	C═O in Ester (-COO)	Stretching	Strong	1750–1730	PU, PU-CNT
1718	Urethane C═O or Ester COO	Stretching	Strong	1725–1705	MDI
1653	Urethane C═O	Stretching	Strong	1680	PU, PU-CNT
1598	Aromatic C═C	Stretching	Medium-weak	1600–1475	PU, PU-CNT, MDI
1539	Amide N-H (-CONH)	Bending	Medium-Strong	1640–1550	PU, PU-CNT
1413	Alkane C-H	Bending	Medium	1450–1375	PU, PU-CNT
1379	Methyl CH_3	Bending	Medium	1450–1375	PU, PU-CNT
1349	Amine C-N	Stretching	Medium-strong	1350–1000	PU, PU-CNT
1307	C-O (Esther)	Stretching	Strong	1300–1000	PU, PU-CNT
1224	C-O (Esther)	Stretching	Strong	1300–1000	PU, PU-CNT
1067	C-O (Esther)	Stretching	Strong	1300–1000	PU, PU-CNT
946	Aromatic C-H	Out-of-plane bending	Strong	1000–650	PU, PU-CNT, MDI
810	Aromatic C-H	Out-of-plane bending	Strong	1000–650	PU, PU-CNT, MDI
753	Aromatic C-H	Out-of-plane bending	Strong	1000–650	PU, PU-CNT, MDI

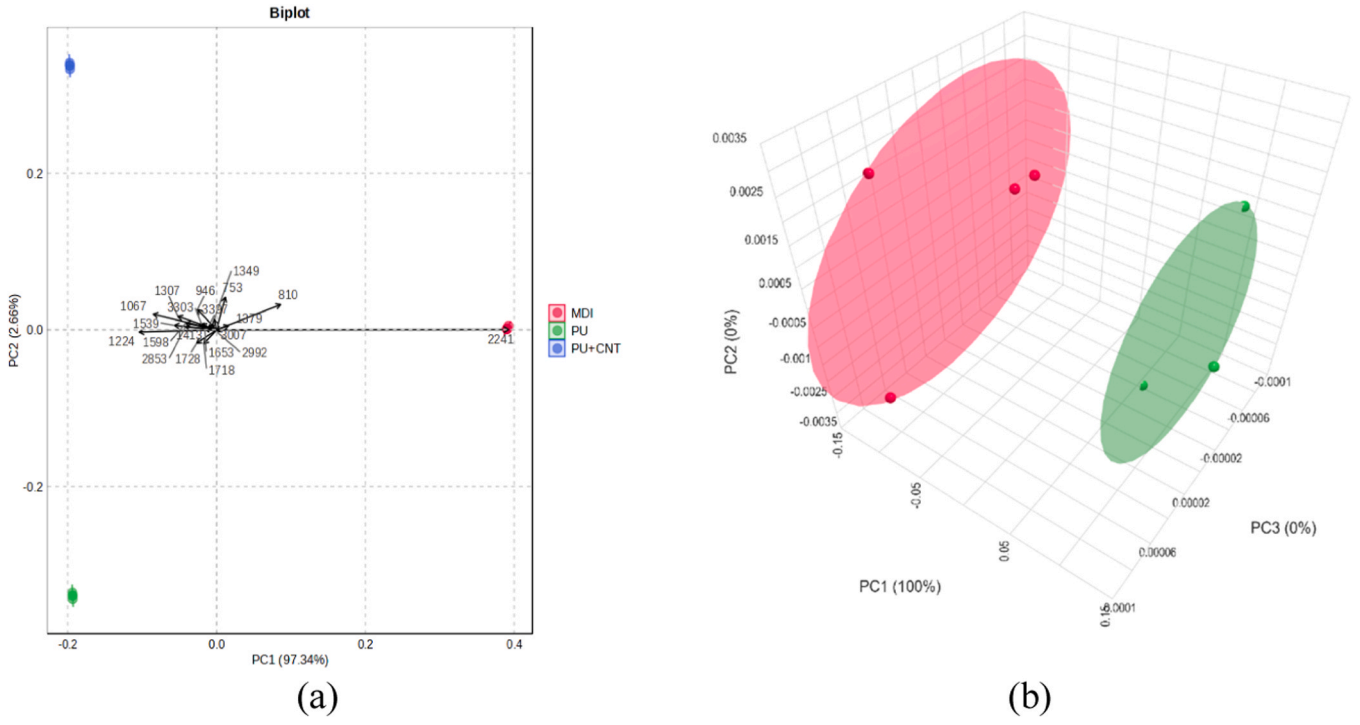

Fig. 2. (a) PCA Biplot of MDI, PU, and PU-CNT; (b) PCA Biplot of PU and PU-CNT (Green nodes indicate PU-CNT samples and red nodes indicate PU samples).

visualized in the heatmap analysis (Fig. 3). Among these, peaks at 946 cm^{-1} and 1349 cm^{-1} (within the fingerprint region), as well as a prominent band at 3394 cm^{-1}, showed significant intensity variations. These observations align with previous findings that carbon nanotubes (CNTs) interact preferentially with carbonyl (C═O) groups rather than with N–H groups in the polyurethane matrix [33] The reduced intensity at 3394 cm^{-1} in PU-CNT composites suggests that hydrogen bonding involving N–H groups is partially disrupted, likely due to physical interactions between CNTs and the carbonyl groups, which are more accessible and chemically favorable for weak bonding.

Despite these differences, the overall FTIR spectra of PU and PU-CNT remain largely similar in terms of peak positions and wavenumbers. This consistency confirms that no new covalent bonds are formed between CNTs and the PU matrix. The interaction is predominantly physical adsorption, as further supported by morphological evidence from field emission scanning electron microscopy (FESEM), which shows CNTs embedded within the PU matrix without evidence of chemical bonding [32].

These findings also highlight the potential of FTIR spectroscopy, especially when integrated with multivariate calibration methods such as Partial Least Squares Regression (PLSR) or Principal Component Regression (PCR), as a reliable analytical tool for quantifying PU-to-PU/CNT conversion. By correlating spectral features with CNT content, future studies may validate FTIR as a rapid, cost-effective, and environmentally sustainable method for monitoring CNT incorporation in PU composites. This approach offers significant advantages for real-time

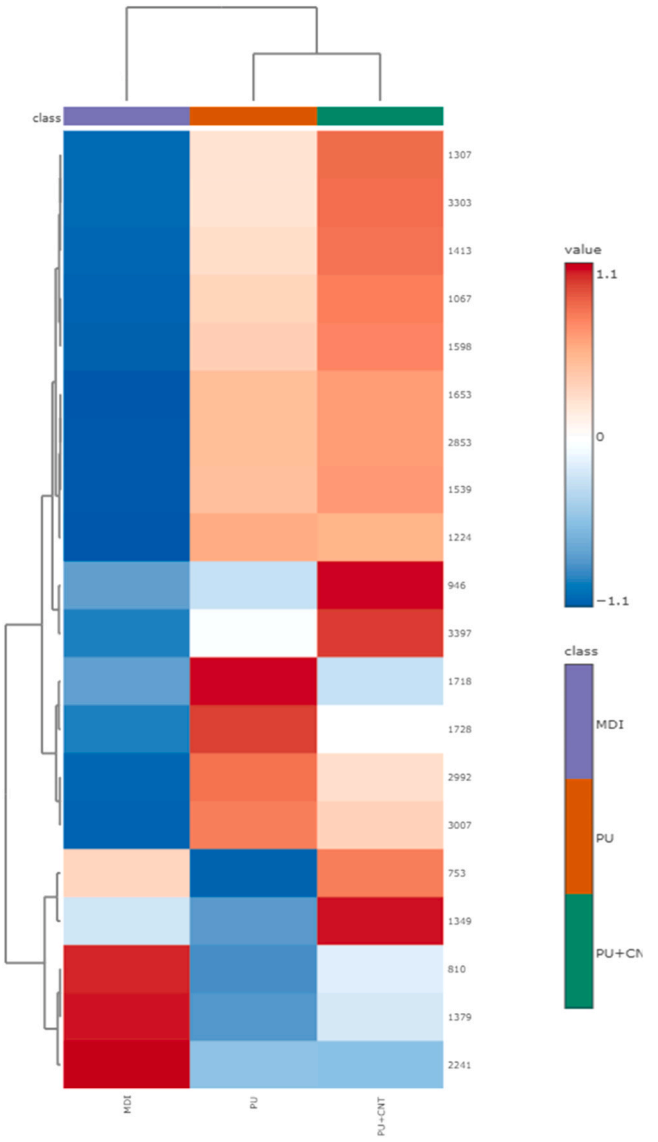

Fig. 3. Heatmap visualization of MDI, PU, and PU-CNT.

quality control and material verification in both research and industrial applications Asghari et al. [36].

To complement the chemical characterization obtained from FTIR, Field Emission Scanning Electron Microscopy (FESEM) was employed to examine the surface morphology of the PU and PU/CNT composite coatings (Fig. 4).

The FESEM micrographs, captured at magnifications ranging from 200 × to 5000 × , offer valuable insights into both the film-forming quality of the polymer matrix and the dispersion behavior of carbon nanotubes within it. Across all samples, the images reveal a relatively uniform, continuous, and smooth surface morphology, indicating effective polymerization and good film integrity. The absence of significant surface defects or agglomerations suggests that the incorporation of CNTs did not disrupt the film formation process. Instead, CNTs appear to be well dispersed within the matrix, likely due to the compatibility between the carbon nanomaterials and the bio-based PU system (Smirnov and Manevitch et al. [37]). This homogeneous morphology underscores the success of the synthesis approach in producing high-quality, defect-minimized coatings, even with the inclusion of nanofillers.

A closer examination of Fig. 4b, which corresponds to the PU/CNT composite, reveals the presence of discrete particulate features dispersed within the polymer surface. These features are not observed in the pristine PU sample and are therefore attributed to the embedded carbon nanotubes. The visible distribution indicates a reasonable level of dispersion; however, some agglomeration is likely, owing to the inherent tendency of carbon nanotubes (CNTs) to cluster via van der Waals forces (Smirnov and Manevitch et al. [37]). These intermolecular forces can result in the formation of agglomerates or bundles, where similar nanotubes self-assemble into highly ordered, crystalline structures, as illustrated in Fig. 4b.

A study also reported the PU/multi-walled carbon nanotube (MWCNT) nanocomposites, showing the FESEM images demonstrated good dispersion and adhesion of the CNTs to the polymeric matrix, which is essential for improving the composite's mechanical properties [38]. Furthermore, the presence of CNTs, even in small clusters, may play a role in enhancing the surface roughness, thermal stability, and mechanical reinforcement of the PU matrix, as suggested in similar nanocomposite systems (Navidfar and Trabzon et al. [39]). The absence of major voids, cracks, or phase separation further confirms the compatibility of CNTs within the polymer matrix and the success of the dispersion technique employed during synthesis. When combined with FTIR results, the FESEM analysis provides visual confirmation of the nanocomposite formation. While FTIR confirmed chemical integration, FESEM supports the physical distribution and morphological stability imparted by CNT incorporation into the PU coating matrix. To evaluate the thermal performance of pure polyurethane (PU) and PU/carbon nanotube (PU/CNT) composites, both thermogravimetric analysis (TGA) and differential scanning calorimetry (DSC) were conducted. These techniques provide insight into decomposition behavior, thermal transitions, and the impact of CNT incorporation on polymer stability. Fig. 5a presents the derivative thermogravimetric (DTG) curves of PU, PU/CNT, and CNT samples, with weight loss data summarized in Table 2.

Pure PU begins thermal decomposition between 250–280°C, initially due to moisture and low molecular weight volatiles. A major degradation event occurs from 320 to 400°C, attributed to the breakdown of urethane linkages in the soft segments, resulting in a sharp 40–50 % mass loss. A secondary degradation stage follows between 400–480°C, associated with the decomposition of hard segments derived from methylene diphenyl diisocyanate (MDI). By 500°C, over 90 % of PU mass is lost, leaving minimal char residue, indicative of limited thermal resistance. In contrast, CNTs exhibit excellent thermal stability, with negligible degradation below 600°C and only modest mass loss (5–10 %) between 600–800°C due to minor oxidative processes. The high residual mass (~90 %) highlights their structural integrity and resistance to thermal breakdown [40].

The PU/CNT composite demonstrates superior thermal performance. Decomposition onset is delayed to ~280–300°C, and degradation proceeds more gradually from 350 to 450°C. This shift reflects the insulating effect of CNTs, which restrict polymer chain mobility and act as thermal barriers [41]. Furthermore, the composite retains 20–30 % of its mass at 800°C, confirming enhanced char formation and structural reinforcement. These improvements support the role of CNTs as effective thermal stabilizers in nanocomposite systems [42].

Principal Component Analysis (PCA) was used on the comprehensive DTG dataset across all temperatures to discern certain temperature points that distinguish CNT from PU and PU/CNT (Fig. 6a) and to differentiate PU from PU/CNT (Fig. 6b). Four critical temperatures were identified to differentiate CNT from PU and PU/CNT, characterized by the highest PC1 contribution along the x-axis, namely 53–185°C (eigenvalue of −0.067 to −0.068), 235–278°C (eigenvalue of 0.067), 398–408°C (eigenvalue of 0.067–0.068), and 700–795°C (eigenvalue of −0.065 to −0.068). PC1 accounts for 71.7 % of the explained variance, while the addition of PC2 results in a cumulative explanation of 100 % variance. At 53–185°C, CNT exhibits significant weight loss in this range relative to PU and PU/CNT. This indicates that CNT may be releasing surface-adsorbed moisture, solvents, or small contaminants. At

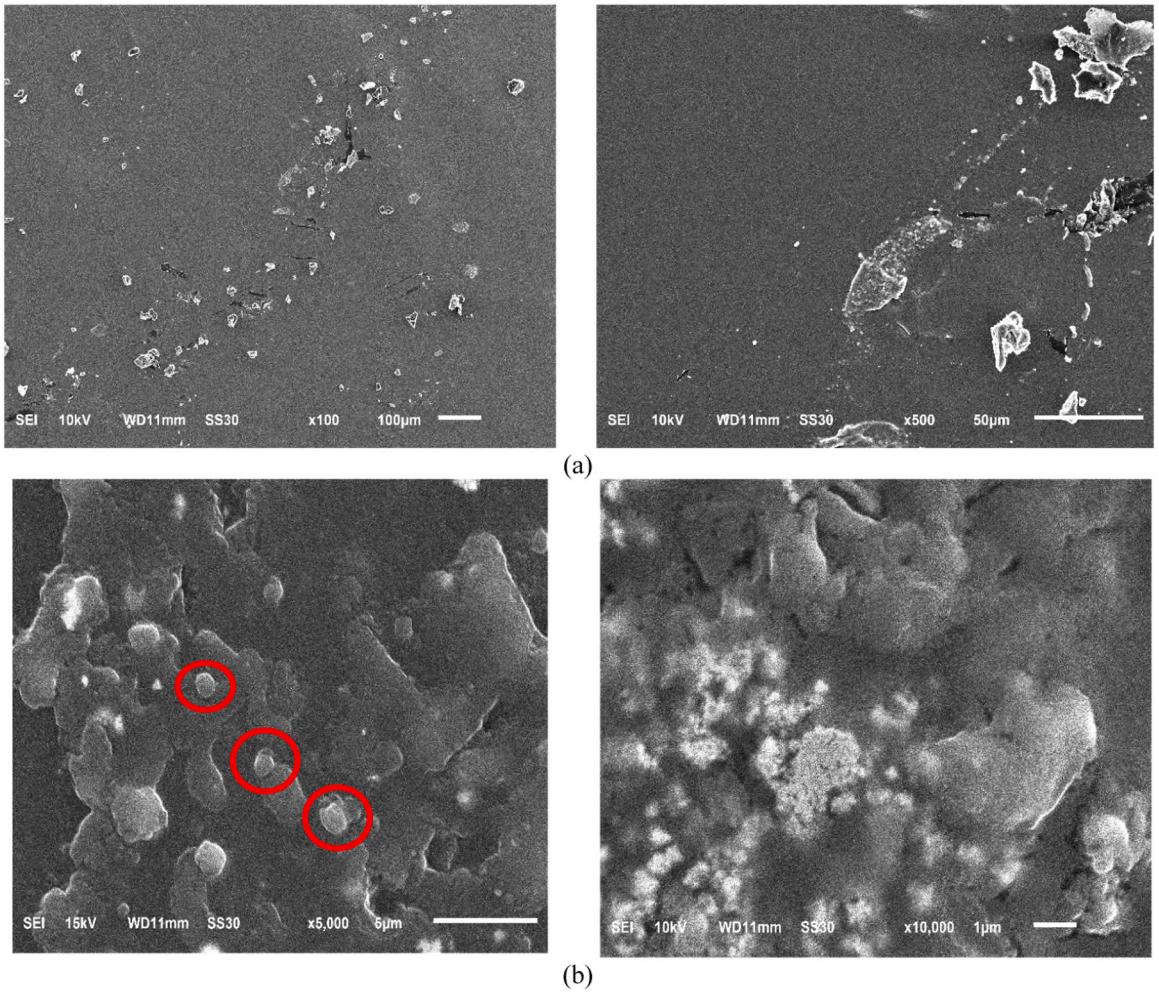

Fig. 4. The micrographs of (a) PU and (b) PU/CNT film were analyzed by the FESEM.

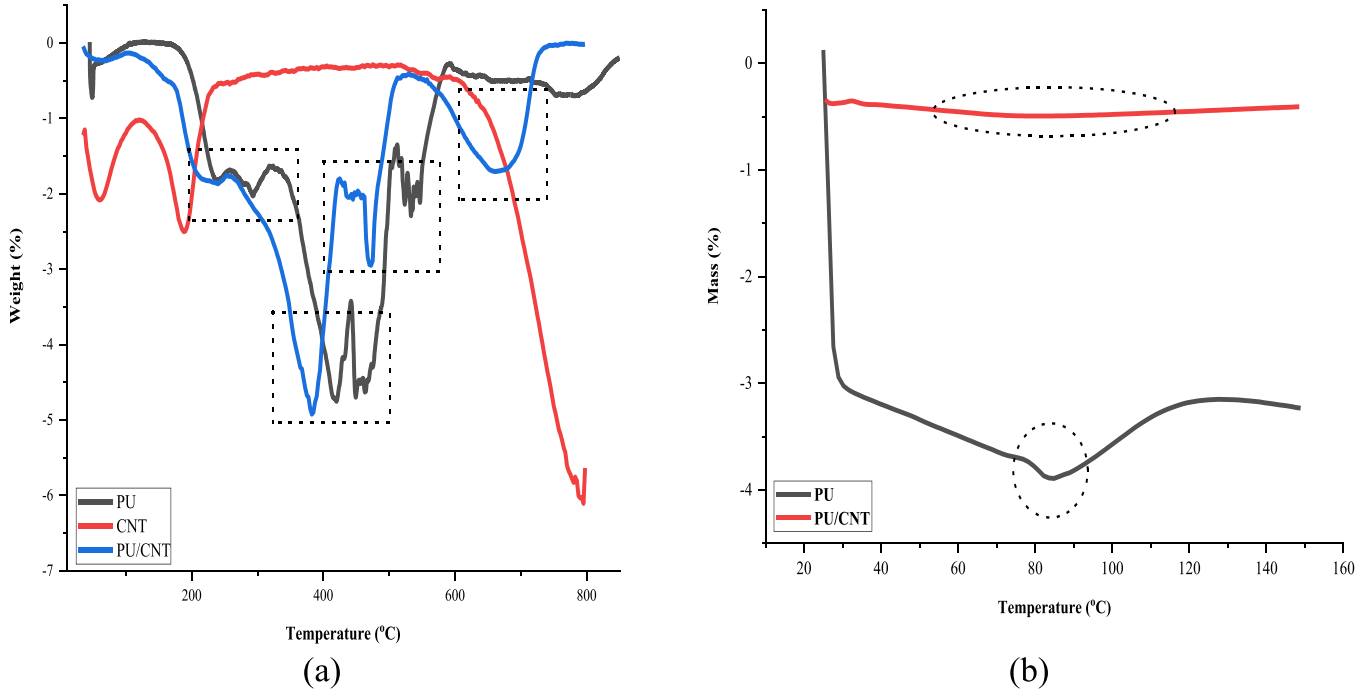

Fig. 5. (a) TGA thermograms of PU, PU/CNT, and CNT, and (b) DSC thermograms of PU and PU/CNT composites.

Table 2
The percentage of weight loss (%).

Temperature range (°C)	PU Weight Loss (%)	PU/CNT Weight Loss (%)	CNT Weight Loss (%)
< 250	~0–5 %	~0–3 %	~0 %
250–400	~50–60 %	~35–45 %	~0 %
400–600	~30–40 %	~20–30 %	~5 %
600–800	~5–10 % residue	~20–30 % residue	~90 % residue

235–278°C, PU and PU/CNT exhibit considerable weight loss, indicating polymer softening and partial degradation, while CNT remains stable. A significant weight loss for PU and PU/CNT was recorded at 398–408°C, indicating the primary degradation phase for both materials. At 700–795°C, CNT exhibits a steady weight loss, indicating carbon-based structural alterations at elevated temperatures, whereas PU and PU/CNT have already undergone degradation, resulting in low residue, but CNT maintains substantial mass due to its carbon composition (Fig. 5a).

The thermal degradation of PU was compared to that of PU/CNT using PCA. PC1, which distinguished PU from PU/CNT along the x-axis (Fig. 6B), was influenced by nearly all temperature ranges: 88–230°C (eigenvalue of 0.058), 280–398°C (eigenvalue of 0.058), 400–570°C (eigenvalue of −0.058), 578–715°C (eigenvalue of 0.058), and 720–795°C (eigenvalue of −0.058). The consistent eigenvalues exhibiting both positive and negative variations indicate that the incorporation of CNT results in a systematic shift, as uniform eigenvalues imply equal contributions from each temperature. At temperatures ranging from 88 to 230°C, CNT may promote the release of moisture or the evaporation of residual solvents, resulting in initial weight loss of the polyurethane/carbon nanotube (PU/CNT) composite. At temperatures ranging from 280 to 398°C, CNT likely alters heat absorption and distribution, facilitating a more rapid onset of degradation. At temperatures ranging from 400 to 570°C, most PU has already experienced degradation, while significant degradation of PU/CNT composites is postponed until 578–715°C. DTG and TGA data collectively delineate the decomposition behavior of PU and PU/CNT by monitoring mass loss trends, degradation rates, and systematic thermal shifts; however, they do not elucidate the thermal transitions that occur in the absence of mass loss. Analyzing the DSC profile of PU and PU/CNT allows for the assessment of how CNT influences phase transitions, thermal stability before degradation, and energy absorption characteristics, thereby providing a comprehensive thermal characterization.

Differential scanning calorimetry (DSC) results, shown in Fig. 5b, further illustrate the impact of CNT incorporation on thermal transitions. For pure PU, a thermal event between 30–60°C corresponds to moisture loss and low molecular volatiles. A subtle inflection near 85°C is attributed to the glass transition temperature (T_g), marking the transition from a glassy to a rubbery state. The T_g is influenced by the presence of MDI-based hard segments, which enhance the rigidity of the polymer [43]. A minor increase beyond 100°C may be due to internal chain rearrangements or typical instrumental noise in subtle transition zones [44]. In comparison, the PU/CNT composite displays a markedly flatter DSC profile across the same temperature range. The negligible mass loss (<0.5 %) and absence of sharp transitions indicate superior moisture resistance and enhanced matrix stability. CNTs appear to suppress moisture diffusion and volatilization of low molecular weight components, an effect consistent with prior findings in PU-based nanocomposites [45].

The thermal transition behavior of the samples was further assessed through DSC analysis (Fig. 5b), with emphasis on glass transition temperature (T_g), moisture evaporation, and initial crystallization behavior. In the case of pure PU, a significant thermal event occurs between 30–60°C, primarily due to the evaporation of absorbed moisture and low molecular weight volatiles. A gradual mass loss continues up to approximately 85°C, where a minor inflection point suggests the glass transition temperature (T_g) of the polymer. The T_g reflects the transition from a rigid glassy state to a more flexible rubbery phase. The presence of MDI contributes to the formation of hard segments that influence this T_g behavior [43]. Notably, a small upward trend in the thermogram beyond 100°C may be observed, potentially due to internal chain rearrangements or minor instrumental artifacts common in DSC or TGA tests at subtle transitions [44]. Combined TGA and DSC analyses confirm that CNT integration significantly improves the thermal stability, char formation, and decomposition resistance of PU. These enhancements make PU/CNT composites promising candidates for applications requiring long-term thermal durability and stability.

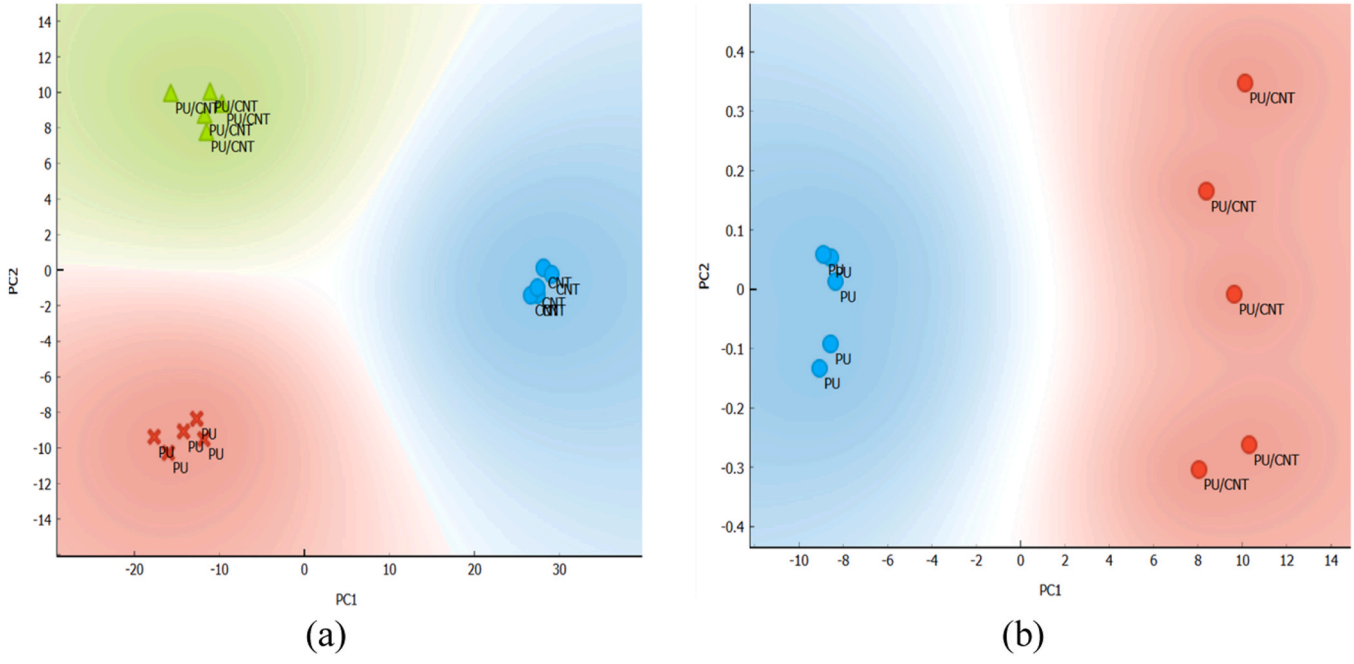

Fig. 6. Principal component analysis visualization utilizing derivative weight data: (a) Differentiation of CNT from PU and PU/CNT, and (b) Comparison between PU and PU/CNT.

The polyurethane (PU) film exhibited a tensile strength of 8.53 MPa, elongation at break of 43.34 %, and a modulus at 100 % strain of 222.10 MPa, indicating good mechanical performance suitable for use as a structural substrate. PU properties depend strongly on formulation: polyols impart chain flexibility and elasticity, whereas methylene diphenyl diisocyanate (MDI) forms rigid, crosslinked hard segments that increase stiffness and deformation resistance. Incorporating carbon nanotubes (CNTs) affected the tensile behavior, with 1 wt% CNT showing the most significant improvement over neat PU, consistent with previous findings where 1 wt% multi-walled CNTs increased tensile stress to ~19.25 MPa and elongation to ~700 %, attributed to uniform dispersion, strong interfacial bonding, and effective reinforcement [46]. At 3–5 wt% CNT, tensile strength gains of ~34 % and substantial improvements in electrical conductivity were reported, though agglomeration began to reduce mechanical uniformity (Huang et al. [47]). Beyond 5 wt%, modulus increases up to 20,000 % and tripled tensile strength has been observed, but elongation dropped to ~2.5 %, highlighting the trade-off between stiffness and flexibility [48]. These results suggest that 1 wt% CNT offers optimal reinforcement for balancing strength, ductility, and conductivity, while higher loadings risk brittleness due to CNT agglomeration.

Verification of electrochemical behavior and conductivity enhancements of the developed coatings, Electrochemical Impedance Spectroscopy (EIS) was performed on pure polyurethane (PU) and PU/CNT composites containing varying CNT loadings (1 %, 2 %, 5 %, and 10 %). The experiments were conducted in phosphate-buffered saline (PBS, 0.01 mol·L^{-1}, pH 7.2) and analyzed using the *Zviewer Analyzer*, which provided Nyquist plots and calculated bulk resistance (Rb) values by fitting the data to a validated Randles circuit model.

As shown in Fig. 7, all samples exhibit the characteristic impedance response of electrochemical systems, namely, a semicircular arc in the high-frequency region (indicative of charge transfer resistance) followed by a linear tail at low frequencies (suggesting Warburg impedance from ionic diffusion). These features confirm that the coating system behaves in accordance with the Randles equivalent circuit, commonly used to describe electrode/electrolyte interfaces [49].

The Nyquist plot for pure PU displays the largest semicircle diameter, signifying the highest Rb value and confirming the inherently insulating nature of polyurethane. However, with the incremental addition of CNTs (1 %, 2 %, 5 %, and 10 %), a clear trend emerges, where the semicircle diameter progressively shrinks, indicating a systematic reduction in bulk resistance. This trend is attributed to the formation of percolated conductive pathways within the PU matrix, as carbon nanotubes begin to interconnect and facilitate electron transport (Al-Safawi [50]). The improvements are especially prominent at higher CNT loadings (5–10 %), where the network density is sufficient to enable more continuous electron conduction throughout the polymer film. This phenomenon is consistent with percolation theory and has been observed in similar conductive polymer nanocomposite systems [51].

Furthermore, the Zviewer circuit modeling corroborates the experimental data, quantitatively showing decreased Rb values and enhanced conductivity as CNT content increases. These results reinforce the dual role of CNTs: not only do they improve mechanical and thermal properties (as discussed in previous sections), but they also substantially enhance the electrical performance of the polymer matrix [52].

The data firmly establish that although pristine PU is electrochemically inert, the incorporation of CNTs transforms it into a functionally conductive composite material, suitable for potential applications in flexible electronics, anti-corrosion coatings, sensors, or bioelectronic devices where a combination of flexibility, durability, and conductivity is required [53].

5. Conclusion

The incorporation of CNTs into a bio-based polyurethane (PU) matrix significantly improved thermal stability, electrical conductivity, and morphological characteristics, confirming the multifunctional potential of these composites. FTIR, supported by principal component analysis (PCA), verified successful CNT integration without altering the core PU structure, while PCA provided a powerful means of distinguishing PU, PU/CNT, and MDI through characteristic absorbance patterns. Application of PCA to TGA data further enabled clear differentiation of thermal degradation profiles, demonstrating its effectiveness as an advanced analytical tool beyond conventional methods. FESEM confirmed uniform CNT dispersion, contributing to enhanced interfacial interactions, while DSC/TGA showed delayed decomposition and higher char yield, indicating improved thermal resistance. Additionally, EIS results revealed the formation of continuous conductive networks at

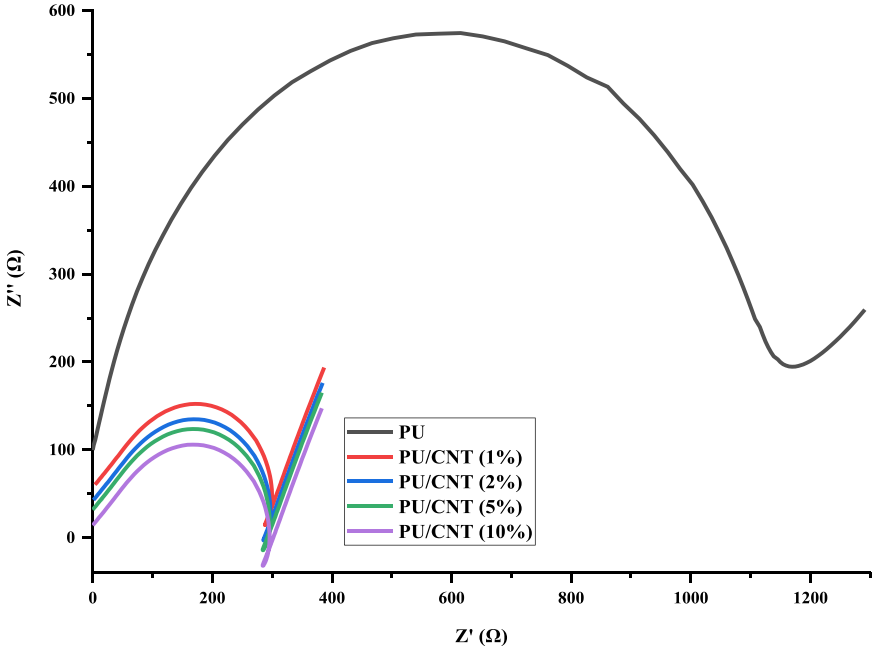

Fig. 7. Electrochemical Impedance Spectroscopy (EIS) spectra of PU and PU/CNT coatings.

higher CNT loadings, underscoring the composites' suitability for applications requiring electrical functionality. Overall, this study not only demonstrates the enhanced performance of PU/CNT composites but also highlights PCA as a novel approach for multivariate analysis of polymer nanocomposites, providing deeper insight into structure–property relationships.

Declaration of Competing Interest

The authors declare that they have no known competing financial interests or personal relationships that could have appeared to influence the work reported in this paper.

Acknowledgments

The authors express their utmost gratitude to Universiti Malaysia Sarawak (UNIMAS) for providing research facilities and technical support via the International Matching Grant (INT/F07/UNS/86787/2025). The authors also thank the Research Group of Solid-State Chemistry and Catalysis, Sebelas Maret University, for providing research facilities.

References

[1] Z. Latif, M. Ali, E.J. Lee, Z. Zubair, K.H. Lee, Thermal and mechanical properties of nano-carbon-reinforced polymeric nanocomposites: a review, J. Compos. Sci. 7 (2023) 441–475.
[2] G. Wang, M. Wang, M. Zheng, B. Ebo, C. Xu, Z. Liu, L. He, Thermoplastic polyurethane/carbon nanotube composites for stretchable flexible pressure sensors, ACS Appl. Nano Mater. 6 (11) (2023) 9865–9873.
[3] R. Li, L. Xia, P. Lyu, J. Zhang, Y. Wang, B. Deng, C. Zhang, X. Liu, W. Xu, High content filling, toughness, and conductive performance of thermoplastic polyurethane/carbon nanotubes composites prepared by constructing the compact interface, Compos. Commun. 28 (2021) 100948.
[4] H.K. Jahromi, A. Farzin, E. Hasanzadeh, S.E. Barough, N. Mahmoodi, M.R. H. Najafabadi, M.S. Farahani, K. Mansoori, S. Shirian, J. Ai, Enhanced sciatic nerve regeneration by poly-L-lactic acid/multi-wall carbon nanotube neural guidance conduit containing Schwann cells and curcumin-encapsulated chitosan nanoparticles in rat, Mater. Sci. Eng. C 109 (2020) 110564.
[5] M.A. Munir, F. Rahmawati, J.A. Jamal, E. Rahmawati, F.Z. Fajriyaningsih, F. R. Putri, A. Gunawan, Fabrication and characterization of new bio-based electrode polyurethane: diverse conducting materials impacts such as graphene oxide, gold, and carbon nanotube, Green. Chem. Lett. Rev. 17 (1) (2024) 2355235.
[6] Z.E. Zadeh, A. Solouk, M. Shafieian, M.H. Nazarpak, Electrospun polyurethane/carbon nanotube composites with different amounts of carbon nanotubes and almost the same fiber diameter for biomedical applications, Mater. Sci. Eng. C 118 (2021) 111403.
[7] A.A. Javidparvar, R. Naderi, B. Ramezanzadeh, Epoxy-polyamide nanocomposite coating with graphene oxide as cerium container generating effective dual active/barrier corrosion protection, Compos. Part B Eng. 172 (2019) 363–375.
[8] R. Goyal, K. Goyal, Development of CNT reinforced Al2O3-TiO2 coatings for boiler tubes to improve hot corrosion resistance, J. Electrochem. Sci. Eng. 12 (5) (2022) 937–945.
[9] M.A. Munir, K.H. Badri, L.H. Heng, A. Inayatullah, H.A. Badrul, E. Emelda, E. Dwinta, N. Kusumawardani, A.S. Wulandari, V. Aprilia, R.B.Y. Supriyono, Design and synthesis of conducting polymer bio-based polyurethane produced from palm kernel oil, Int. J. Polym. Sci. 2022 (1) (2022) 1–13.
[10] K.R. Gajbhiye, B.P. Chaudhari, V.B. Pokharkar, A. Pawar, V. Gajbhiye, Stimuli-responsive biodegradable polyurethane nano-constructs as a potential triggered drug delivery vehicle for cancer therapy, Int. J. Pharm. 588 (2020) 119781.
[11] M. Alam, M. Altaf, N. Ahmad, Rapeseed oil gallate-amide-urethane coating material: Synthesis and evaluation of coating properties, ePolymers 22 (2022) 190–202.
[12] F. Dong, X. Yang, L. Guo, Y. Qian, P. Sun, Z. Huang, X. Xu, H. Liu, A tough, healable, and recyclable conductive polyurethane/carbon nanotube composite, J. Colloid Interface Sci. 631 (2023) 239–248.
[13] X. Jin, J. Wang, X. Dai, L. Liu, Y. Li, Y. Yang, Y. Cao, W. Wang, H. Wu, S. Guo, Flame-retardant poly(vinyl alcohol)/MXene multilayered films with outstanding electromagnetic interference shielding and thermal conductive performances, Chem. Eng. J. 380 (2020) 122475.
[14] Q. Qi, L.I. Ma, B. Zhao, S. Wang, X. Liu, Y. Lei, C.B. Park, An effective design strategy for the sandwich structure of PVDF/GNP-Ni-CNT composites with remarkable electromagnetic interference shielding effectiveness, ACS Appl. Mater. Interfaces 12 (32) (2020) 36568–36577.
[15] K. Goyal, H. Singh, R. Bhatia, Effect of carbon nanotubes on properties of ceramics based composite coatings, Adv. Eng. Forum 26 (2018) 53–66.
[16] R. Ravindren, S. Mondal, P. Bhawal, S.M.N. Ali, N.C. Das, Superior electromagnetic interference shielding effectiveness and low percolation threshold through the preferential distribution of carbon black in the highly flexible polymer blend composites, Polym. Compos. 40 (4) (2019) 1404–1418.
[17] J. Ju, T. Kuangm, X. Ke, M. Zeng, Z. Chen, S. Zhang, X. Peng, Lightweight multifunctional polypropylene/carbon nanotubes/carbon black nanocomposite foams with segregated structure, ultralow percolation threshold and enhanced electromagnetic interference shielding performance, Compos. Sci. Technol. 193 (2020) 108116.
[18] B. Wei, L. Zhang, S. Yang, Polymer composites with expanded graphite network with superior thermal conductivity and electromagnetic interference shielding performance, Chem. Eng. J. 404 (2021) 126437.
[19] C. Li, X.L. Zeng, L.Y. Tang, Y.M. Yao, D.L. Zhu, R. Sun, J.B. Xu, C.P. Wong, Three-dimensional interconnected graphene microsphere as fillers for enhancing thermal conductivity of polymer, Chem. Eng. J. 368 (2019) 79–87.
[20] X. Pan, L. Shen, A.P.H.J. Schenning, C.W.M. Bastiaansen, Transparent, high-thermal-conductivity ultradrawn polyethylene/graphene nanocomposite films, Adv. Mater. 31 (40) (2019) 1904348.
[21] J. Tolvanen, J. Hannu, M. Hietala, K. Kordas, H. Jantunen, Biodegradable multiphase poly (lactic acid)/biochar/graphite composites for electromagnetic interference shielding, Compos. Sci. Technol. 181 (2019) 107704.
[22] J.H. Cai, X.H. Tang, X.D. Chen, M. Wang, Temperature and strain-induced tunable electromagnetic interference shielding in polydimethylsiloxane/multi-walled carbon nanotube composites with temperature-sensitive microspheres, Comp. Part A Appl. Sci. Manufac. 140 (2020) 106188.
[23] B. Shin, S. Mondal, M. Lee, S. Kim, Y.I. Huh, C. Nah, Flexible thermoplastic polyurethane-carbon nanotube composites for electromagnetic interference shielding and thermal management, Chem. Eng. J. 418 (2021) 129282.
[24] M.A. Munir, J.A. Jamal, M.M. Said, S. Ibrahim, M.S. Ahmad, Polyurethane application to transform screen-printed electrode for rapid identification of histamine isolated from fish, Scientifica 2023 (2023) 1, 5444256.
[25] J. Demsar, T. Curk, A. Erjavec, C. Gorup, T. Hocevar, M. Milutinovic, M. Mozina, M. Polajnar, M. Toplak, A. Staric, M. Stajdohar, L. Umek, L. Zagar, J. Zbontar, M. Zitnik, B. Zupan, Orange: data mining toolbox in python, J. Mach. Learn. Res. 14 (2013) 2349–2353.
[26] J.R. Beattie, F.W.L. Esmonde-White, Exploration of principal component analysis: deriving principal component analysis visually using spectra, Appl. Spectrosc. 75 (4) (2021) 361–375.
[27] M.A. Munir, A. Inayatullah, The chemometric approach for verification of paracetamol level in pharmacies products using spectrophotometer UV-Vis, ASM Sci. J. 19 (2024) 1–15.
[28] J. Shen, X. Li, B. Shentu, Exploring thermodynamic and structural properties of carbon nanotube/thermoplastic polyurethane nanocomposites from atomistic molecular dynamics simulations, RSC Adv. 13 (2023) 21080–21087.
[29] Y. Ozaki, Infrared spectroscopy—mid-infrared, near-infrared, and far-infrared/terahertz spectroscopy, Anal. Sci. 37 (2021) 1193–1212.
[30] D. Yang, J.K. Brett, M.C. Celina, Hydrolysis of poly(ester urethane): in-depth mechanistic pathways through FTIR 2D-COS spectroscopy, Polym. Degrad. Stab. 231 (2025) 111094.
[31] I. Lukaszewska, A. Bukowczan, K.N. Raftopoulos, K. Pielichowski, Water-polymer interactions and mechanisms of water-driven glass transition decrease in non-isocyanate polyhydroxyurethanes with varying hydration sites, Polymer 302 (2024) 127060.
[32] S.S. Nordi, E.E.M. Noor, C.K. Kok, N.M. Julkapli, M.F. Baig, Phase, Chemical, Thermal, and Morphological Analyses of Thermoplastic Polyurethane (TPU) Nanocomposites Reinforced with Jute Cellulose Nanofibers (CNFs), Polymers 17 (7) (2025) 899.
[33] J. Xue, D. Liu, D. Li, T. Hong, C. Li, Z. Zhu, Y. Sun, X. Gao, L. Guo, X. Shen, P. Ma, Q. Zheng, New Carbon Materials for Multifunctional Soft Electronics, Adv. Mater. 37 (2) (2025) 2312596.
[34] W. Si, S. Zhang, The green manufacturing of thermoplastic starch for low-carbon and sustainable energy applications: a review on its progress, Green. Chem. 26 (2024) 1194–1222.
[35] C. Xia, Y. Li, T. Fei, W. Gong, Facile one-pot synthesis of superhydrophobic reduced graphene oxide-coated polyurethane sponge at the presence of ethanol for oil-water separation, Chem. Eng. J. 345 (2018) 648–658.
[36] A. Asgahri, M.K. Khorrami, A.B. Garmarudi, Comparison between partial least square and support vector regression with a genetic algorithm wavelength selection method for the simultaneous determination of some oxygenate compounds in gasoline by FTIR spectroscopy, Infrared Phys. Technol. 105 (2020) 103177.
[37] V.V. Smirnov, L.I. Manevitch, Carbon nanotubes in arrays: competition of Van-der-Waals and elastic forces, Dokl. Phys. 64 (5) (2019) 218–221.
[38] Y.N. Gupta, T. Bhave, A. Chakraborty, A.K. Pandey, R.B. Sharma, D.K. Setua, Nonisothermal crystallization kinetics of carbon nanotubes containing segmented polyurethane elastomer, Polym. Eng. Sci. 56 (11) (2016) 1248–1258.
[39] A. Navidfar, L. Trabzon, Fabrication and characterization of polyurethane hybrid nanocomposites: mechanical, thermal, acoustic, and dielectric properties, Emergent Mater. 5 (4) (2022) 1157–1165.
[40] Y. Yao, H. Lu, Mechanical properties and failure mechanism of carbon nanotube concrete at high temperatures, Constr. Build. Mater. 297 (2021) 123782.
[41] J. He, J. Chen, L. Shi, Q. Li, W. Lu, S. Qu, W. Qiu, G. Zhou, Fabrication of thermally robust carbon nanotube (CNT)/SiO 2 composite films and their high-temperature mechanical properties, Carbon 147 (2019) 236–241.
[42] H.L. Shi, H. Zhang, J.N. Wang, L.Q. Wan, F.R. Huang, On line construction of carbon nanotube/polytriazole composite films with high tensile and heat resistant properties, Carbon 218 (2024) 118726.

[43] J. Jiang, Z. Lu, J. Shen, T. Wada, H. Kato, M. Chen, Decoupling between calorimetric and dynamical glass transitions in high-entropy metallic glasses, Nat. Commun. 12 (1) (2021) 3843.
[44] R. Dai, A.K. Gangopadhyay, R.J. Chang, K.F. Kelton, A method to predict the glass transition temperature in metallic glasses from properties of the equilibrium liquid, Acta Mater. 172 (2019) 1–5.
[45] B.S. Lucic, M. Zeljko, R.M. Kraljic, Influence of multiwalled carbon nanotube modification on polyurethane properties: II. mechanical properties, electrical conductivity and thermal stability, J. Chem. Chem. Eng. 66 (5-6) (2017) 241–248.
[46] H. Xia, M. Song, Preparation and characterization of polyurethane–carbon nanotube composites, Soft Matter 1 (5) (2005) 386–394.
[47] X. Huang, Y. Mo, W. Wu, M. Ye, C. Hu, Preparation and properties of waterborne polyurethane/carbon nanotube/graphene/cellulose nanofiber composites, Processes 12 (9) (2024) 1913.
[48] P. Kalakonda, S. Banne, P.B. Kalakonda, Enhanced mechanical properties of multiwalled carbon nanotubes/thermoplastic polyurethane nanocomposites, Nanomater. Nanotechnol. 9 (2019).
[49] L. Stolz, M. Winter, J. Kasnatscheew, Practical relevance of charge transfer resistance at the Li metal electrode|electrolyte interface in batteries? J. Solid State Electrochem. (2024).
[50] S. Al-sawafi, A theoretical study on the behaviour of strain conductivity in carbon nanotube/high-density polyethylene composites, Pramana J. Phys. 98 (2) (2024) 77.
[51] J. Payandehpeyman, M. Mazaheri, A.S. Zeraati, S. Jamasb, U. Sundararaj, Physics-based modeling and experimental study of conductivity and percolation threshold in carbon black polymer nanocomposites, Appl. Compos. Mater. 31 (1) (2024) 127–147.
[52] X. Yan, L. Qiao, H. Tan, H. Tan, C. Liu, K. Zhu, Z. Lin, S. Xu, Effect of carbon nanotubes on the mechanical, crystallization, electrical and thermal conductivity properties of CNT/CCF/PEKK Composites, Materials 15 (14) (2022) 4950.
[53] Z.Z. Eivazi, A. Solouk, M. Shafieian, N.M. Haghbin, Electrospun polyurethane/carbon nanotube composites with different amounts of carbon nanotubes and almost the same fiber diameter for biomedical applications, Mater. Sci. Eng. C. 118 (2021) 111403.